Technical Note

Landslides (2024) 21:155–163
DOI 10.1007/s10346-023-02144-1
Received: 29 March 2023
Accepted: 5 September 2023
Published online: 19 September 2023

Tommaso Carlà · Giovanni Gigli · Luca Lombardi · Massimiliano Nocentini · Lorenz Meier · Lino Schmid · Susanne Wahlen · Nicola Casagli

Real-time detection and management of rockfall hazards by ground-based Doppler radar

Abstract Rockfalls are ubiquitous products of landscape evolution in steep mountainous terrains. Among other effects, they pose a significant concern to the management of transportation corridors located on valley floors. Here, we describe the field application of a ground-based Doppler radar that performs real-time, long-range, wide-area detection and tracking of rockfalls and related slope hazards. We deployed the instrument at the Ruinon landslide, where accelerated deformation of upper chaotic debris has for several months promoted secondary mass wasting processes of extremely rapid velocity. In particular, large rolling boulders had the potential to propagate beyond the toe of the landslide and impact a road that connects important localities in the Italian Alps interiors. The Doppler radar was programmed to actuate a pair of traffic lights so that a predefined exclusion zone could instantly be enforced for approaching vehicles upon initial movement detection. We discuss the setup of the alarm system, the main observations collected during the monitoring campaign, and how this technique may enhance safety in areas critically exposed to rockfalls as well as our understanding of rockfall dynamics in general.

Keywords Ground-based Doppler radar · Rockfall · Real-time alarms · Extremely rapid landslides

Introduction

Although often limited in volume, rockfalls are responsible for a major percentage of landslide-induced casualties due to their high velocity, frequency, and unpredictability (Guzzetti et al. 2004). Risk mitigation and control strategies may be designed based on a variety of investigative approaches: for example, indexes of rockfall susceptibility are derived from the orientation of rock mass discontinuities intersecting the rock face (Gigli et al. 2014, 2022; Matasci et al. 2018); numerical procedures allow the assessment of block-specific failure probability and mechanism through limit equilibrium or stress–strain analyses (Stead et al. 2006; Paronuzzi et al. 2016) or simulate the runout behavior of the detachable mass (Agliardi and Crosta 2003; Lan et al. 2007; Volkwein et al. 2011); remote measurement of displacement precursors occasionally provides a foundation for early-warning protocols of comparatively large-scale failures (Carlà et al. 2019). These are valuable information, but ultimately it is not possible to pinpoint the whereabouts, timing, and magnitude of all future rockfalls at a certain site. In reality, many of the factors governing rockfalls are of intrinsic stochastic nature (Frattini et al. 2008; Wang et al. 2014), and kinematic release of source blocks will typically involve negligible accumulations of detectable damage and deformation (Fig. 1a, b).

Roads in steep mountainous terrains may be constrained to follow the floor of narrow valleys, with no alternative routes available to circumvent areas markedly prone to rockfalls. In given circumstances, the unfavorable combination of topographic setting and expected scale of events means that there are no feasible slope stabilization works (e.g., rock scaling, blasting) or defense structures (e.g., rock sheds, barriers, embankments) ensuring adequate protection—or at least, these remedial measures may not be readily undertaken after identification of new or previously overlooked hazards. In the last few years, in an attempt to enhance safety in this kind of scenarios, there has been a growing interest in the development of ground-based Doppler radar instrumentations specifically devoted to rockfall monitoring (Meier et al. 2016; Michelini et al. 2020); however, practical applications in the field are yet to be documented.

We deployed one of such devices to manage rockfall hazards at the Ruinon landslide, a ~30 million m^3 highly disaggregated rockslide in the Central Italian Alps. The landslide experienced phases of accelerated deformation in 2019 and 2020, escalating into surface velocities persistently greater than 1 m/day. This coincided with a remarkable increase in rockfall activity, which threatened to disrupt an important road at lower elevations. The ground-based Doppler radar helped bridge two conflicting needs: keeping the road open to avoid isolation of a nearby town and, during occurrence of a rockfall, preventing vehicles from entering the area at risk (i.e., the area that could be affected by the propagation of rockfalls). We present an overview of the implemented alarm system and of the outputs from observed events, thus highlighting key operational features as well as scientific perspectives related to use of the technique.

Operating principles

The Doppler radar object of this work performs real-time, long-range, wide-area detection and tracking of rockfalls and related slope hazards. Similar instruments have been aimed at studying the propagation of snow avalanches (Gauer et al. 2007; Vriend et al. 2013) or the activity of volcanic edifices (Vöge and Hort 2009; Valade et al. 2012). The rationale behind the intended use of the technique is justified by the discrete character of rockfall hazards affecting mountainous roads—either no rockfall is occurring and vehicles may safely travel along the segment of road at risk or a rockfall is occurring and an exclusion zone should be enforced locally. In the latter case, evacuation may effectively be achieved by stopping vehicles outside the boundaries of the potential runout area as soon as a rockfall originates. The assumption holds true if the travel time of the rockfall from kinematic release to intersection with the road is longer than the approximate travel time of a vehicle

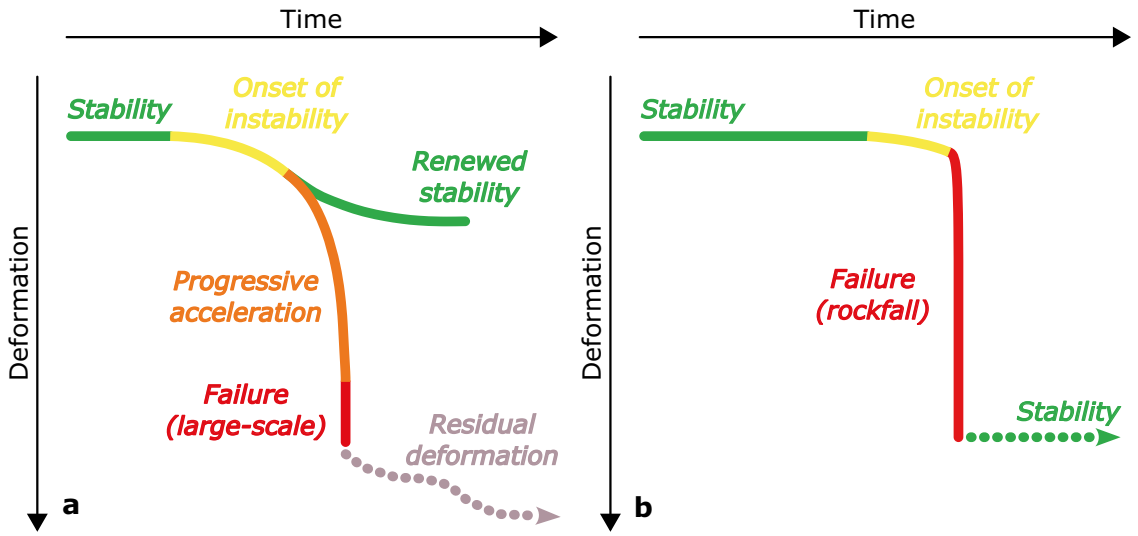

Fig. 1 Schematic diagram of **a** accelerating rock slope deformation leading to comparatively large-scale failures as opposed to **b** negligible precursors to small-scale failures (rockfalls)

from one side to the other of the predefined exclusion zone and vehicles do not stop or proceed at exceedingly slow speed within the predefined exclusion zone. If the rockfall does not propagate far enough to reach the road, traffic may promptly be restored at the conclusion of the event.

The main module consists of an FMCW (Frequency-Modulated Continuous-Wave) Doppler radar operating in the X-band at a base frequency of 10 GHz and a bandwidth of 40 MHz. It is equipped with a transmitting antenna and two receivers so as to retrieve the angular position of the targets (i.e., pixels) through direction-of-arrival estimation. The transmitted and reflected signals have different frequencies because of the initial frequency modulation, which can be exploited to determine the distance (i.e., range) of a moving target with respect to the Doppler radar. An additional Doppler processing yields spectra of all moving targets within the field of view (vertical and horizontal angular aperture of 30°). A confusion matrix analysis, developed on the basis of large training datasets from several rockfall sites (Meier et al. 2016), iteratively classifies these spectra and distinguishes movement from actual events while filtering the contribution of irrelevant sources (e.g., atmospheric effects, oscillation of tree crowns). Further refinement can be obtained by feeding data from events at the specific site of interest. The extent of the Doppler shift generated by a moving target is a complex function of the line-of-sight velocity, particle size distribution, and relative position of the rockfall. In broad terms, the instrument is normally run at a sensitivity that is suitable for spotting an object of ~ 1 m^3 moving at a distance of ~ 1 km at line-of-sight velocities of several meters per second. Detection occurs within seconds from the onset of the event, and distinct objects may be tracked separately as long as their offset is higher than ~5 m in range and is equivalent to more than ~3° in azimuth (i.e., ~10 m at common operative ranges). Final heat maps of Doppler shift "intensity" are georeferenced during post-processing by means of a GNSS unit to outline the area hit by the rockfall. This dimensionless parameter is proportional to the amplitude of the echo power from every moving target at every range and azimuth bin, integrated over the whole rockfall event. The central processing unit also communicates the real-time activation/deactivation of alarms through dedicated output ports, to which up to four alarm devices can be connected. Compatible alarm devices include traffic lights, sirens, or rising arm barriers. As with any radar instrumentation, monitoring can be carried out independently of sunlight and weather (e.g., also during darkness and periods of low visibility caused by rainfall, snowfall, or fog). The components must be mounted on a pole with a precast concrete base or similar fixed support.

Activity of the Ruinon landslide and setup of the rockfall alarm system

The Ruinon landslide dislocates ~30 million m^3 of metamorphic rock and chaotic debris on the right flank of the Frodolfo River Valley in the Upper Valtellina (Central Italian Alps), currently extending from just above the slope toe up to an elevation of ~2100 m (Fig. 2). Geomorphological expressions of a larger deep-seated gravitational slope deformation (DSGSD), believed to have been primarily conditioned by glacial debuttressing and WNW–ESE trending structural constraints (Agliardi et al. 2001), are found up to elevations ~900 m higher. The basic features of the Ruinon landslide are in good agreement with the description of "translational rock-debris slides" by Glastonbury and Fell (2008): it involves heavily fractured pre-Permian phyllites from the Upper Austroalpine crystalline basement down to a depth between 50 and 70 m, overlain by a 10–20 m thick incoherent layer of variably sized disoriented boulders in a gravelly to silty–clayey matrix (Fig. 3). The slide area is dissected by two major scarps (termed "upper" and "lower" scarps based on relative elevation) characterized by decametric height drops and planimetric length of several hundreds of meters. Debris has accumulated throughout the slide area (Fig. 4a) in response to the retrogression of these scarps, incorporation of previously intact ground, and bedrock disaggregation from internal shearing, progressive damage, and weathering. Extremely rapid mass

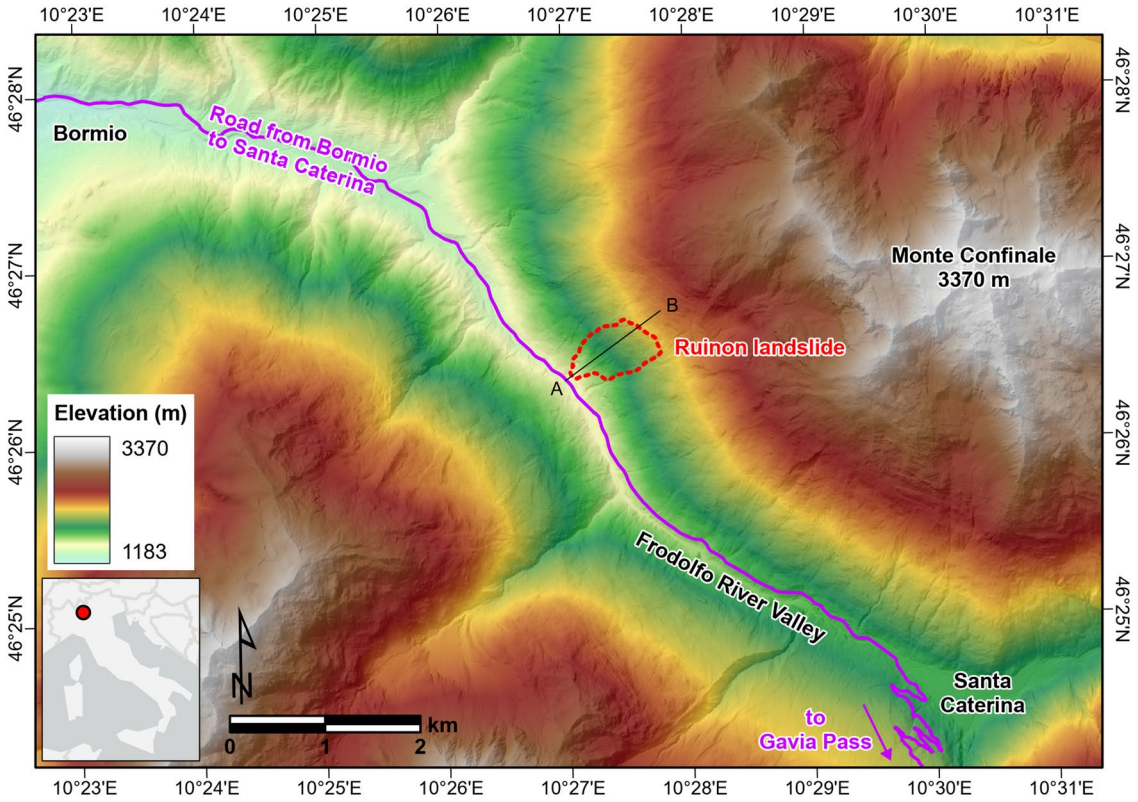

Fig. 2 Map of the Frodolfo River Valley with location of the road from Bormio to Santa Caterina and the approximate outline of the Ruinon landslide. The AB line marks the trace of the cross section in Fig. 3

wasting processes in the form of secondary rockfalls are directly promoted by remobilization of the upper debris. Large displacements may in fact dig out individual boulders—some of which range up to tens or even hundreds of cubic meters in volume—from below the ground surface and allow their kinematic release (Fig. 4b). They may also create locally unstable slope geometries, leading to shallow slumps and more fragmental falls.

The Upper Valtellina has a continental-alpine climate, with rainfalls concentrated in the summer and autumn. Slope deformation at Ruinon has been observed to develop intermittently under the influence of this seasonality (Crosta and Agliardi 2003; Del Ventisette et al. 2012). Crosta et al. (2017) and Carlà et al. (2021) suggested that reactivation phases of the landslide, whose intensity and duration have tended to increase since at least the late 1990s, are closely linked to pore water pressure perturbations resulting from a complex combination of rainfall infiltration and deep groundwater recharge. Measurements from two standpipe piezometers installed near the upper scarp have shown that piezometric levels often rise to their yearly peak between the months of June and July, when heavy rainfalls are concurrent with (or shortly follow) melting of the winter snow cover at higher elevation (Carlà et al. 2021). Such kind of conditions propelled a reactivation phase of exceptional intensity and duration in the summer of 2019, during which a vast debris-covered area downslope of the lower scarp (red shaded polygon in Fig. 4a) attained velocities persistently in excess of 1 m/day and rockfalls occurred at much higher rates than previously witnessed.

The evolution of the Ruinon landslide heavily impacts a road that runs alongside the Frodolfo River. This can be the only route enabling vehicles to access the popular tourist town of Santa Caterina at the upper end of the valley (Fig. 2). A backup route is represented by the Gavia Pass (elevation 2652 m), which is cleared of snow for only few months per year. At the time of the landslide reactivation in the summer of 2019, a mixed 5 m high embankment and concrete barrier bordered the segment of road at risk for rockfalls; however, large rolling boulders could build up sufficient kinetic energy to render any protective structure ineffective. A precedent was in this sense established in August 2019, when a ~65 m^3 block of rock landed on the road after breaking through a section of concrete barrier (Fig. 4c). On the other hand, the majority of rockfalls would be confined to higher slopes and stop before entering the catch ditch at the slope toe.

In July 2020, because of renewed large seasonal displacements, a Doppler radar was installed on the left flank of the valley to continuously monitor the highly active slide area downslope of the lower scarp (Fig. 5a, b). Two traffic lights were placed at the edges of the embankment and connected to the central processing unit via fiber-optic cabling. Figure 6a, b illustrates the alarm triggering logic: the field of view of the instrument was divided into a "region of interest" (ROI), corresponding to the debris-covered slopes from which rockfalls were most likely to originate, and a "danger zone" (DZ), between the catch ditch and the protruding debris lobe. Since it could not be known a priori if a spotted falling object would eventually reach the road, the radar was programmed

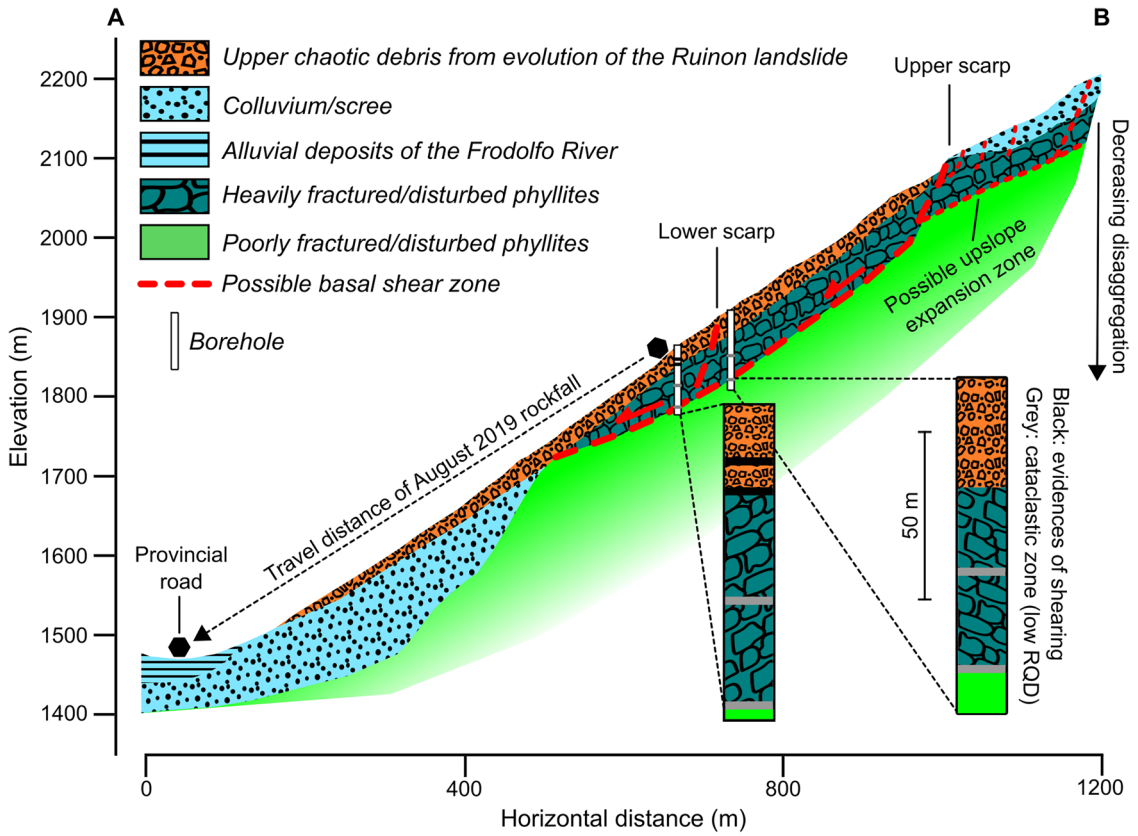

Fig. 3 Updated schematic cross section of the Ruinon landslide (adapted from Carlà et al. 2021). Note that the distal edge of the upper layer of chaotic debris produced by the evolution of the landslide was located at an elevation ~200 m higher prior to the beginning of the reactivation phase in the summer of 2019

to enforce an exclusion zone (i.e., switch the traffic lights to red) at the instant the event detection threshold is first surpassed. A heat map of Doppler shift intensity is then produced once movement has ceased, from which it is determined whether only the region of interest or also the danger zone has been affected by the rockfall. In the former case, the radar switches the traffic lights back to green with a delay of 90 s (granted that no further events occur during this interval); otherwise, a user-controlled reset is required pending appraisal of the integrity of the road and embankment. The reset could be carried out in situ or from a web-based interface, where event data were uploaded together with images from a network of optical cameras overlooking the slope. Authorities responsible of managing the road were informed of changes of status information via automated e-mail and short message service (SMS).

Summary of outputs

Here, we report on the main rockfall events detected by the Doppler radar between July and December 2020. By the end of this period, surface drainage works performed around the slide area resulted in a strong reduction of slope displacements, and concurrently, rockfall occurrence became sporadic again. Out of a total of 60 rockfalls that triggered an alarm, three of them propagated far enough to enter the catch ditch at the slope toe—and in each case they stopped short of colliding with the embankment. Figure 7a–d shows the heat maps of Doppler shift intensity for these long-runout rockfalls and for a short-runout rockfall that originated from the lower scarp, at notably greater range. For visual verification of the radar outputs against the actual rockfall trajectories, video recordings from an optical camera installed above the instrument (Fig. 5b) are available as Online Resources 1–4. The heat map of Doppler shift intensity in Fig. 7d is of particular interest, as it reproduces the bifurcated trajectory of the two distinct boulders forming this rockfall. Table 1 lists the time of onset, time of issued alarm, volume, duration, and runout parameters (i.e., range, runout, and average velocity, as outputted by the Doppler radar) for the selected events. It is specified that the time of onset of the rockfall matches the timestamp when movement is first noticed in video recordings; duration is the number of seconds between the time the Doppler radar issued the alarm and the time the falling boulder finally came to rest; range is the distance between the Doppler radar and the rockfall source area; and runout is the distance traveled along the slope by the rockfall. Duration, volume (when available), and runout parameters refer to the boulder that first detached from the slope in the two cases that the rockfall consisted of more than one falling boulder—this being also the one that traveled farther along the slope.

Figure 8 details the number of true detections with time alongside the number of false detections stemming from atmospheric effects (primarily during rainstorms), compared to the daily precipitation and the cumulative displacements of a representative point within the highly active slide area—slope

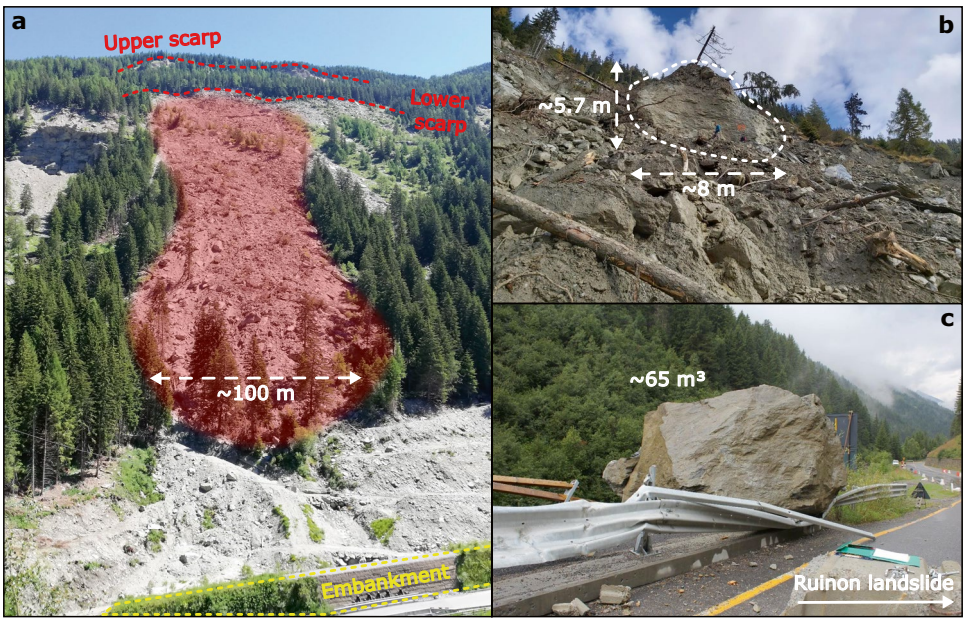

Fig. 4 **a** Frontal photo of the Ruinon landslide, taken in July 2020 from the Doppler radar installation site (see Fig. 5a). The red shaded polygon marks the highly active slide area, where surface velocities persistently exceeded 1 m/day. Note that the concrete barrier damaged by the August 2019 rockfall had by this time been replaced by a new (unvegetated in the photo) section of embankment. **b** Example of a large precarious boulder that was rapidly brought to surface in October 2020 by slope displacements ~100 m downslope of the lower scarp. **c** Close-up photo (looking toward the opposite valley side with respect to the Ruinon landslide) of the ~65 m^3 boulder that damaged the road to Santa Caterina in August 2019

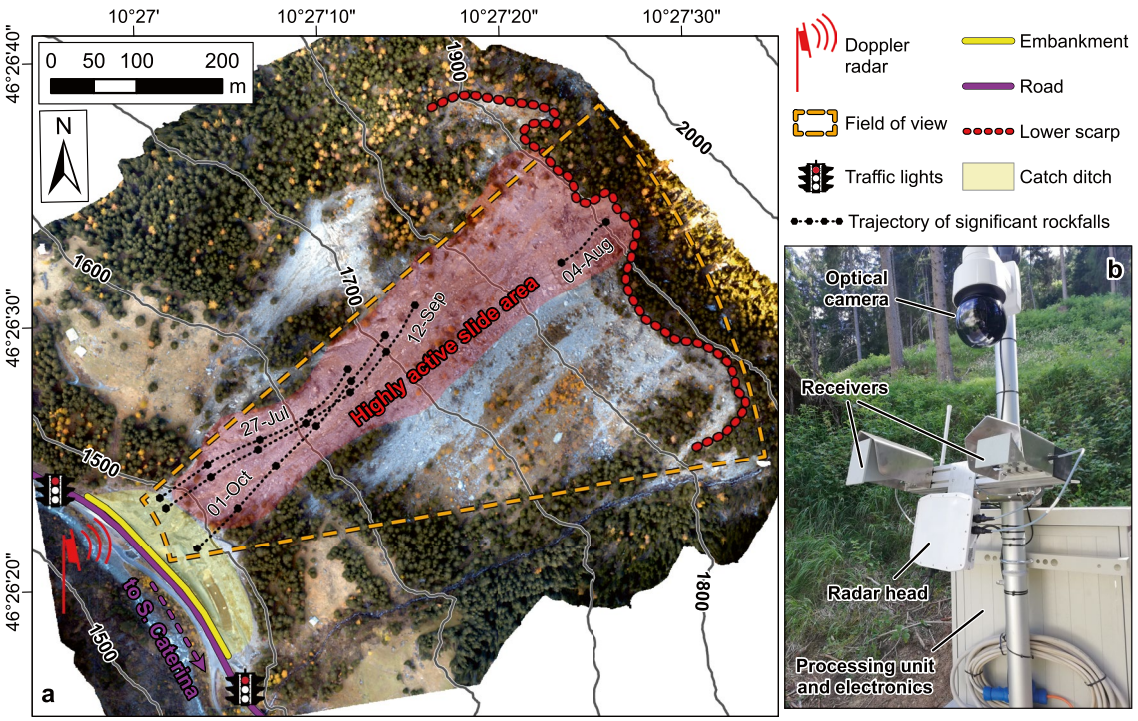

Fig. 5 **a** Plan view of the slide area downslope of the lower scarp with location of the components of the rockfall alarm system and **b** close-up photo of the radar instrumentation. The approximate trajectory and day of occurrence of four significant rockfalls detected during the monitoring campaign (described later in the manuscript) are indicated to illustrate the segment of road at higher risk. The background ortophoto in (**a**) was acquired in October 2020 by drone photogrammetry (courtesy of ARPA Lombardia)

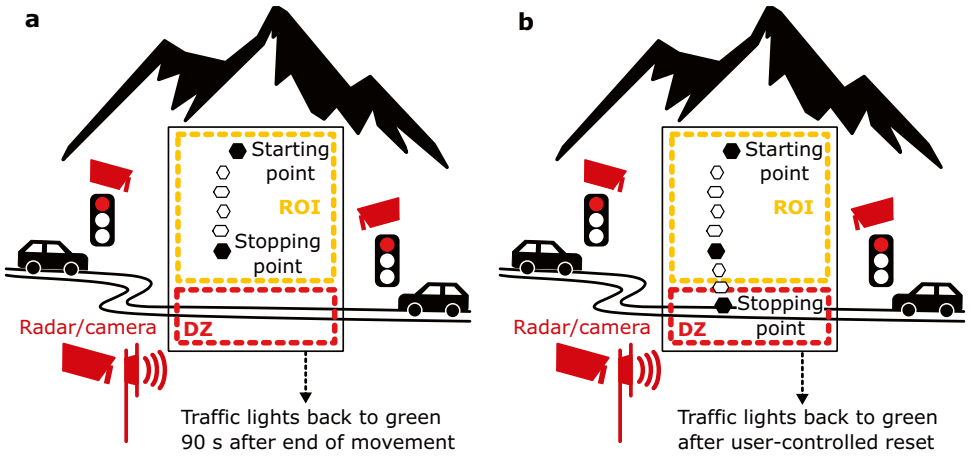

Fig. 6 Alarm triggering logic for managing rockfall hazards at the Ruinon landslide. The traffic lights are instantly switched to red upon initial movement detection; once this has ceased, the road may be reopened **a** automatically if the event affected only the region of interest (ROI) on higher slopes or **b** manually if it propagated into the danger zone (DZ) at the slope toe. Note that, in the former case, any preferred interval may be set as precautionary delay before the traffic lights are switched back to green

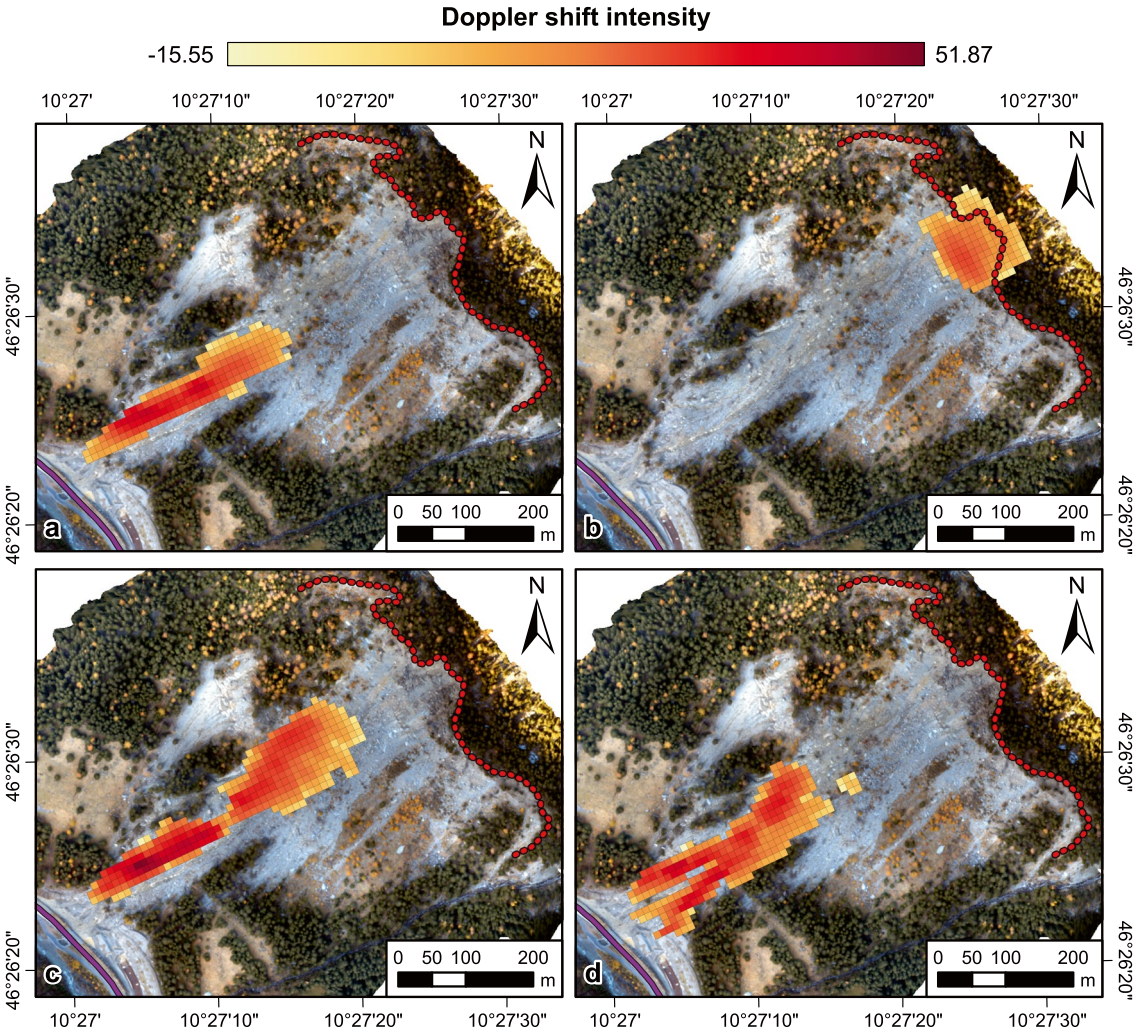

Fig. 7 Heat maps of Doppler shift intensity (see text for explanation) resulting from selected significant rockfalls occurred during the monitoring campaign: **a** 27 July 2020; **b** 4 August 2020; **c** 12 September 2020; **d** 1 October 2020. Runout parameters of the events are listed in Table 1; related video recordings are provided in Online Resources 1–4. As in Fig. 5a, the red dashed line and purple solid line define the lower scarp and the road to Santa Caterina, respectively. Note that the bifurcated trajectory of the 1 October 2020 rockfall (Online Resource 4) is correctly captured by the heat map of Doppler shift intensity in (**d**)

Table 1 Characteristics of the rockfall events shown in Figs. 5 and 7. The lag between the time of rockfall onset and the time of issued alarm primarily depends on the line-of-sight distance with the rockfall source area and how quickly the rockfall gained sufficient momentum to exceed the event detection threshold (it will be shorter for increasingly large rockfalls). Values of rockfall volume were estimated in situ

Time of onset	Time of alarm	Approximate volume (m^3)	Duration since alarm (s)	Range (m)	Runout (m)	Average velocity (km/h)
27-Jul-2020 11:49:38	27-Jul-2020 11:49:40	6	36	487	330	33
04-Aug-2020 06:35:44	04-Aug-2020 06:35:49	N.A.*	11	816	105	36
12-Sep-2020 09:58:43	12-Sep-2020 09:58:48	4.5	40	622	434	39
01-Oct-2020 18:18:40	01-Oct-2020 18:18:53	1*	42	532	375	32

*Rockfall consisting of more than one falling boulder

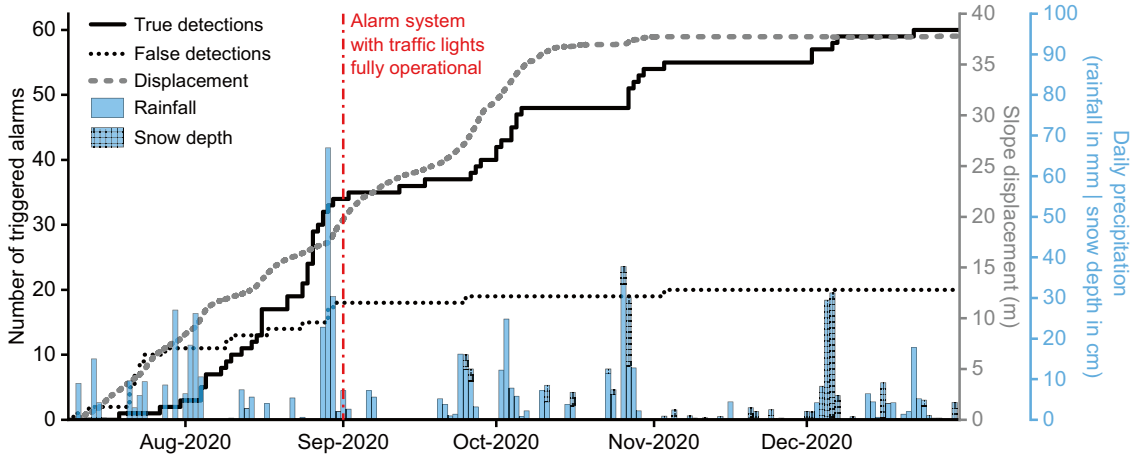

Fig. 8 Time series of rockfall detections (both true and false alarms), daily precipitation, and cumulative slope displacements between July and December 2020. The red dash-dotted line indicates the point up to which the Doppler radar was run at its maximum sensitivity in order to refine the event detection threshold. Slope displacements were measured by a ground-based interferometric synthetic aperture radar (see Carlà et al. 2021). Rainfall was measured by a non-heated tipping bucket rain gauge located ~250 m westward of the slide area, snow depth by an ultrasonic sensor located at an elevation ~500 m higher than the upper scarp (courtesy of ARPA Lombardia)

displacements were measured by a ground-based interferometric synthetic aperture radar and have been recently analyzed by Carlà et al. (2021). In the first 50 days of monitoring, the instrument was purposefully run at its maximum sensitivity to expand the set of captured events (including very low magnitude ones) and refine the algorithms underlying the event detection threshold, hence the initial higher rate of false detections. True and false detections were recognized by examining video recordings and the characteristics of the heat maps of Doppler shift intensity (atmospheric effects tend to produce an irregularly shaped signature spreading over most of the field of view). The alarm system plus the traffic lights became fully operational on 1 September 2020 (red dash-dotted line in Fig. 8). Although explicit correlations may not be determined from this relatively small dataset, it is confirmed that high landslide activity was consistently accompanied by higher rates of rockfall occurrence; when landslide activity decreased in mid-October, rockfalls manifested a pattern more strictly contingent on precipitation (e.g., see detections in late October and early December). This suggests that, regardless of landslide activity, rockfalls may occasionally initiate as the ground adjacent to precarious boulders is softened by rainfall; similarly, boulders already lying precariously on the slope may lose their balance under the weight of accumulated snow. There have been no evidences or accounts of significant rockfalls that traveled down the protruding debris lobe undetected by the instrument.

Discussion and conclusions

The experience gained at the Ruinon landslide indicates that ground-based Doppler radar can accurately track in real time the propagation of rockfalls. This feature may be exploited to limit exposure to rockfall hazards along critical parts of transportation corridors adjacent to steep slopes while maintaining such infrastructures in operation. Inconveniences related to traffic interruption can be minimized by triggering appropriate alarm devices only when a rockfall is actually occurring. However, evacuation from the predefined exclusion zone must be achievable in a shorter time than the expected travel time of a long-runout event. In other words, if a vehicle goes past the first alarm device encountered

along its path just before movement on the slope is detected, it must have sufficient margin to exit the exclusion zone from the opposite side before the rockfall reaches the road. Preliminary modeling of rockfall runout is therefore a necessary prerequisite—to this aim, Doppler radar observations themselves can serve as an objective reference for model validation. At Ruinon, it was estimated that boulders with an average volume of 40 m^3 could build enough momentum to reach the road if they were mobilized at elevations higher than ~1700 m and that corresponding travel times were in the order of at least 30 s. This was approximately 10 s more than the time required for a vehicle traveling at an average speed of 40 km/h to cover the distance between the two traffic lights. Warning panels were positioned along the road to inform road users not to stop or proceed at exceedingly slow speeds within the exclusion zone. Access by pedestrians was also forbidden.

We emphasize that we did not employ prototypical instrumentation, but nowadays this can be obtained similarly to other established remote sensing techniques (e.g., ground-based radar interferometry, terrestrial laser scanning). A downside is certainly the high costs that it still entails. Thanks to the pronounced decrease of landslide activity in early 2021, remedial measures were undertaken including construction of a full earth-reinforced embankment with doubled height (10 m) and blasting of all dangerous boulders lying on the slope. Large buried boulders are in fact brought to the surface much more slowly and much less frequently during phases of lower slope displacements, and they can be blasted well before full kinematic release is approached. After completion of these works, the monitoring campaign was therefore ended.

In principle, the technique may be extended to any extremely rapid landslide of the avalanche or flow type. Calibration of the event detection threshold for hazard management of landslides other than rockfall (e.g., debris flows) would have to be adjusted on hitherto uncollected training datasets (Meier et al. 2016). Even for rockfalls, the procedure may not be straightforward in topographically complex and/or highly vegetated scenarios. A too sensitive setting may improve detection capability of smaller events but likewise increase the likelihood of false alarms (especially under the disturbance of adverse weather), hence impairing confidence in the alarm system. Falling objects are ideally best tracked over regular and bare ground surfaces such as rock walls and talus slopes. Importantly, these are the most common sources of rockfall hazards for roads in mountainous terrains.

In addition to its strictly operational use, long-term monitoring by ground-based Doppler radar could enhance our quantitative understanding of the fundamental patterns of rockfalls. These have been explored through indirect observational methods relying on the compilation of inventories or the back-analysis of isolated, well-documented events; that is, being highly unpredictable and discrete in time, rockfalls are rarely assessed as they occur, rather they are assessed after they have occurred based on evidences left in the field (Luckman 2013). Instead, ground-based Doppler radar provides a means to collect empirical observations on rockfall initiation, propagation, and deposition at high resolution and without systemic censoring. Interpretation of these temporally and spatially ordered records could serve multiple purposes. Robust statistics on source areas, travel distance, and lateral dispersion (Jaboyedoff and Labiouse 2011) could be derived from the density of curvilinear rockfall trajectories extrapolated from maps of Doppler shift intensity. Precise determination of rockfall timing and fluctuations could allow more explicit investigations on both the influence of environmental drivers (e.g., rainfall, freeze–thaw) and how small, frequent events accompany the development of comparatively large instability mechanisms in rock slopes (Rosser et al. 2007; Kromer et al. 2015). Inspection of spotted fallen boulders, or of corresponding scars in rock slopes, could strengthen the reliability of volume-frequency (Hungr et al. 1999; Williams et al. 2019; Graber and Santi 2022) and probability distributions (Macciotta et al. 2016, 2017; Fei et al. 2023); on the same subject, continuous monitoring could largely reduce the bias induced by superimposition (i.e., adjoining failures being sampled as one) on estimates of local erosional fluxes associated with rockfalls.

Acknowledgements

The ground-based Doppler radar used to monitor the Ruinon landslide was supplied by Geopraevent AG, holder of proprietary ROCYX technology. The authors are grateful to the personnel and authorities of Regione Lombardia, ARPA Lombardia, Comunità Montana Alta Valtellina, Parco Nazionale dello Stelvio, Provincia di Sondrio, Comune di Valfurva, and IDS Georadar who supported this study. ARPA Lombardia kindly provided the ortophoto of the landslide and precipitation measurements.

Declarations

Conflict of interest The authors declare no competing interests.

References

Agliardi F, Crosta G, Zanchi A (2001) Structural constraints on deep-seated slope deformation kinematics. Eng Geol 59:83–102. https://doi.org/10.1016/S0013-7952(00)00066-1

Agliardi F, Crosta G (2003) High resolution three-dimensional numerical modelling of rockfalls. Int J Rock Mech Min Sci 40:455–471. https://doi.org/10.1016/S1365-1609(03)00021-2

Carlà T, Nolesini T, Solari L, Rivolta C, Dei Cas L, Casagli N (2019) Rockfall forecasting and risk management along a major transportation corridor in the Alps through ground-based radar

interferometry. Landslides 16:1425–1435. https://doi.org/10.1007/s10346-019-01190-y
Carlà T, Gigli G, Lombardi L, Nocentini M, Casagli N (2021) Monitoring and analysis of the exceptional displacements affecting debris at the top of a highly disaggregated rockslide. Eng Geol 294:106345. https://doi.org/10.1016/j.enggeo.2021.106345
Crosta GB, Agliardi F (2003) Failure forecast for large rock slides by surface displacement measurements. Can Geotech J 40:176–191. https://doi.org/10.1139/T02-085
Crosta GB, Agliardi F, Rivolta C, Alberti S, Dei Cas L (2017) Long-term evolution and early warning strategies for complex rockslides by real-time monitoring. Landslides 14:1615–1632. https://doi.org/10.1007/s10346-017-0817-8
Del Ventisette C, Casagli N, Fortuny-Guasch J, Tarchi D (2012) Ruinon landslide (Valfurva, Italy) activity in relation to rainfall by means of GBInSAR monitoring. Landslides 9:97–509. https://doi.org/10.1007/s10346-011-0307-3
Fei L, Jaboyedoff M, Guerin A, Noël F, Bertolo D, Derron M-H, Thuegaz P, Troilo F, Ravanel L (2023) Assessing the rock failure return period on an unstable Alpine rock wall based on volume-frequency relationships: the Brenva Spur (3916 m a.s.l., Aosta Valley, Italy). Eng Geol 323:107239. https://doi.org/10.1016/j.enggeo.2023.107239
Frattini P, Crosta G, Carrara A, Agliardi F (2008) Assessment of rockfall susceptibility by integrating statistical and physically-based approaches. Geomorphology 94:419–437. https://doi.org/10.1016/j.geomorph.2006.10.037
Gauer P, Kern M, Kristensen K, Lied K, Rammer L, Schreiber H (2007) On pulsed Doppler radar measurements of avalanches and their implication to avalanche dynamics. Cold Reg Sci Technol 50:55–71. https://doi.org/10.1016/j.coldregions.2007.03.009
Gigli G, Morelli S, Fornera S, Casagli N (2014) Terrestrial laser scanner and geomechanical surveys for the rapid evaluation of rock fall susceptibility scenarios. Landslides 11:1–14. https://doi.org/10.1007/s10346-012-0374-0
Gigli G, Lombardi L, Carlà T, Beni T, Casagli N (2022) A method for full three-dimensional kinematic analysis of steep rock walls based on high-resolution point cloud data. Int J Rock Mech Min Sci 157:105178. https://doi.org/10.1016/j.ijrmms.2022.105178
Glastonbury J, Fell R (2008) Geotechnical characteristics of large slow, very slow, and extremely slow landslides. Can Geotech J 45:984–1005. https://doi.org/10.1139/T08-021
Graber A, Santi P (2022) Power law models for rockfall frequency-magnitude distributions: review and identification of factors that influence the scaling exponent. Geomorphology 418:108463
Guzzetti F, Reichenbach P, Ghigi S (2004) Rockfall hazard and risk assessment along a transportation corridor in the Nera Valley, Central Italy. Env Eng 34:191–208. https://doi.org/10.1007/s00267-003-0021-6
Jaboyedoff M, Labiouse V (2011) Preliminary estimation of rockfall runout zones. Nat Hazards Earth Syst Sci 11:819–828. https://doi.org/10.5194/nhess-11-819-2011
Hungr O, Evans SG, Hazzard J (1999) Magnitude and frequency of rock falls and rock slides along the main transportation corridors of southwestern British Columbia. Can Geotech J 36:224–238. https://doi.org/10.1139/T98-106
Kromer RA, Hutchinson DJ, Lato MJ, Gauthier D, Edwards T (2015) Identifying rock slope failure precursors using LiDAR for transportation corridor hazard management. Eng Geol 195:93–103. https://doi.org/10.1016/j.enggeo.2015.05.012
Lan H, Martin CD, Lim CH (2007) RockFall analyst: a GIS extension for three-dimensional and spatially distributed rockfall hazard modeling. Comput Geosci 33:262–279. https://doi.org/10.1016/j.cageo.2006.05.013
Luckman BH (2013) Processes, transport, deposition, and landforms: rockfall. In: Shroder JF (ed) Treatise on geomorphology, vol 7. Academic Press, San Diego, pp 174–182
Macciotta R, Martin CD, Morgenstern NR, Cruden DM (2016) Quantitative risk assessment of slope hazards along a section of railway in the Canadian Cordillera—a methodology considering the uncertainty in the results. Landslides 13:115–127. https://doi.org/10.1007/s10346-014-0551-4
Macciotta R, Hendry M, Cruden DM, Blais-Stevens A, Edwards T (2017) Quantifying rock fall probabilities and their temporal distribution associated with weather seasonality. Landslides 14:2025–2039. https://doi.org/10.1007/s10346-017-0834-7
Matasci B, Stock GM, Jaboyedoff M, Carrea D, Collins BD, Guérin A, Matasci G, Ravanel L (2018) Assessing rockfall susceptibility in steep and overhanging slopes using three-dimensional analysis of failure mechanisms. Landslides 15:859–878. https://doi.org/10.1007/s10346-017-0911-y
Meier L, Jacquemart M, Blattmann B, Arnold B (2016) Real-time avalanche detection with long-range, wide-angle radars for road safety in Zermatt, Switzerland. In: Proceedings of the 2016 International Snow Science Workshop, 3–7 October. Breckenridge, Colorado, pp 304–308
Michelini, Viviani F, Bianchetti M, Coli N, Leoni L, Stopka CJ (2020) A new radar-based system for detecting and tracking rockfall in open pit mines. In: Dight PM (ed) Proceedings of the 2020 International Symposium on Slope Stability in Open Pit Mining and Civil Engineering, 12–14 May. Australian Centre for Geomechanics, Perth, pp 1183–1192. https://doi.org/10.36487/ACG_repo/2025_79
Paronuzzi P, Bolla A, Rigo E (2016) 3D stress-strain analysis of a failed limestone wedge influenced by an intact rock bridge. Rock Mech Rock Eng 49:3223–3242. https://doi.org/10.1007/s00603-016-0963-7
Rosser N, Lim M, Petley D, Dunning S, Allison R (2007) Patterns of precursory rockfall prior to slope failure. J Geophys Res 112:F04014. https://doi.org/10.1029/2006JF000642
Stead D, Eberhardt E, Coggan JS (2006) Developments in the characterization of complex rock slope deformation and failure using numerical modelling techniques. Eng Geol 83:217–235. https://doi.org/10.1016/j.enggeo.2005.06.033
Valade S, Donnadieu F, Lesage P, Mora MM, Harris A, Alvarado GE (2012) Explosion mechanisms at Arenal volcano, Costa Rica: an interpretation from integration of seismic and Doppler radar data. J Geophys Res 117:B01309. https://doi.org/10.1029/2011JB008623
Vöge M, Hort M (2009) Installation of a Doppler radar monitoring system at Merapi volcano, Indonesia. IEEE Trans Geosci Remote Sens 47:251–271. https://doi.org/10.1109/TGRS.2008.2002693
Volkwein A, Schellenberg K, Labiouse V, Agliardi F, Berger F, Bourrier F, Dorren LKA, Gerber W, Jaboyedoff M (2011) Rockfall characterization and structural protection—a review. Nat Hazards Earth Syst Sci 11:2617–2651. https://doi.org/10.5194/nhess-11-2617-2011
Vriend NM, McElwaine JN, Sovilla B, Keylock CJ, Ash M, Brennan PV (2013) High-resolution radar measurements of snow avalanches. Geophys Res Lett 40:727–731. https://doi.org/10.1002/grl.50134
Wang X, Frattini P, Crosta GB, Zhang L, Agliardi F, Lari S, Yang Z (2014) Uncertainty assessment in quantitative rockfall risk assessment. Landslides 11:711–722. https://doi.org/10.1002/grl.50134
Williams JG, Rosser NJ, Hardy RJ, Brain MJ (2019) The importance of monitoring interval for rockfall magnitude-frequency estimation. J Geophys Res Earth Surf 124:2841–2853. https://doi.org/10.1029/2019JF005225

Supplementary Information The online version contains supplementary material available at https://doi.org/10.1007/s10346-023-02144-1.

Tommaso Carlà (✉) · Giovanni Gigli · Luca Lombardi · Nicola Casagli
Department of Earth Sciences, Università degli Studi di Firenze, Via Giorgio La Pira 4, 50121 Florence, Italy
Email: tommaso.carla@unifi.it

Massimiliano Nocentini
Center for Civil Protection, Università degli Studi di Firenze, Largo Enrico Fermi 2, 50125 Florence, Italy

Lorenz Meier · Lino Schmid · Susanne Wahlen
Geopraevent AG, Technoparkstrasse 1, 8005 Zurich, Switzerland